Supporting Information

Adherence to Bürgi-Dunitz stereochemical principles requires significant structural rearrangements in Schiff base formation: Insights from transaldolase complexes

Samuel H. Light[1,2], George Minasov[1,2], Mark-Eugene Duban[1], and Wayne F. Anderson[1,2]

[1]Center for Structural Genomics of Infectious Diseases, and [2]Department of Molecular Pharmacology and Biological Chemistry, Feinberg School of Medicine, Northwestern University, Chicago, Illinois 60611

*Correspondence to: Wayne F. Anderson, PhD, 303 East Chicago Avenue, Chicago IL, 60611. Phone: (312) 503-1697; Fax: (312) 503-5349; E-mail: wf-anderson@northwestern.edu

Supporting Discussion

11 Supporting Figures

S1. Supporting Discussion

Identification of CT specific induced fit conformational changes
Unexpectedly, a comparison of the five transaldolase structures revealed a systematic set of conformational changes. The differences in F6P and S7P length and in non-covalent versus covalent bound substrate position results in the regular spacing of the substrate phosphate group, spanning a distance of 1.8 Å over the captured reaction states (**Figure S8a)**. Despite this range, similar electrostatic interactions are maintained with the phosphate anion across structures. This feat is accomplished by induced fit conformational changes in the primary phosphate contacting residue, Arg232, and correlated movement of the α9-α10 helix connecting loop that flanks the Arg232 side chain (**Figure S8a**).

A comparison to the TLL structures reveals that these conformational changes – which in effect provide mobility that allows the phosphate binding pocket to adapt to the variable, reaction state-dependent position of the phosphate anion – are specific to the CT transaldolase class. The TLL binding pocket is generally similar to its CT counterpart. The only significant distinction regards the Arg232 (Arg169 in *T. acidophilum* TL) guanidinium group, which is rotated ~90° relative to its CT position. This difference has minimal impact on S7P binding, as Arg232 makes similar interactions (albeit using different nitrogen atoms) with the phosphate in both transaldolase types (**Figure S8b**). A more significant distinction regards the F6P complexes. In the TLL structure Arg232 forgoes conformational change and consequently is too far from the sugar to interact with the F6P phosphate (**Figure S8b**).

Curiously, the distinction in phosphate binding pocket mobility likely relates to the α9-α10 helix connecting loop. Since this loop is one of the CT specific insertions discussed in the introduction (**Figure S3**), TLL lacks a comparable Arg232 flank (**Figure S8b**). The prominent position and striking movement of the loop in CT structures, in conjunction with the correlation between loop presence and arginine mobility illustrated by the two transaldolase types, strongly suggests a crucial role of the loop in facilitating the observed CT specific conformational changes.

The functional significance of these induced fit conformational changes is not entirely clear. Given that TLL remains catalytically proficient, phosphate pocket mobility cannot be essential for activity but rather must exert a more subtle influence over enzyme function. One possibility is that this distinction confers differing relative substrate affinities to the two transaldolase classes. Considering that CT makes favorable electrostatic contacts with both sugar substrates whereas TLL only contacts the longer substrate, CT likely has a higher relative F6P affinity than does TL. Since relative substrate affinity may influence the rate of metabolic flux within the context of a complex biosynthetic pathway, the observed distinctions in substrate binding could significantly affect and functionally differentiate the transaldolase types (Watt and Dean, 2000).

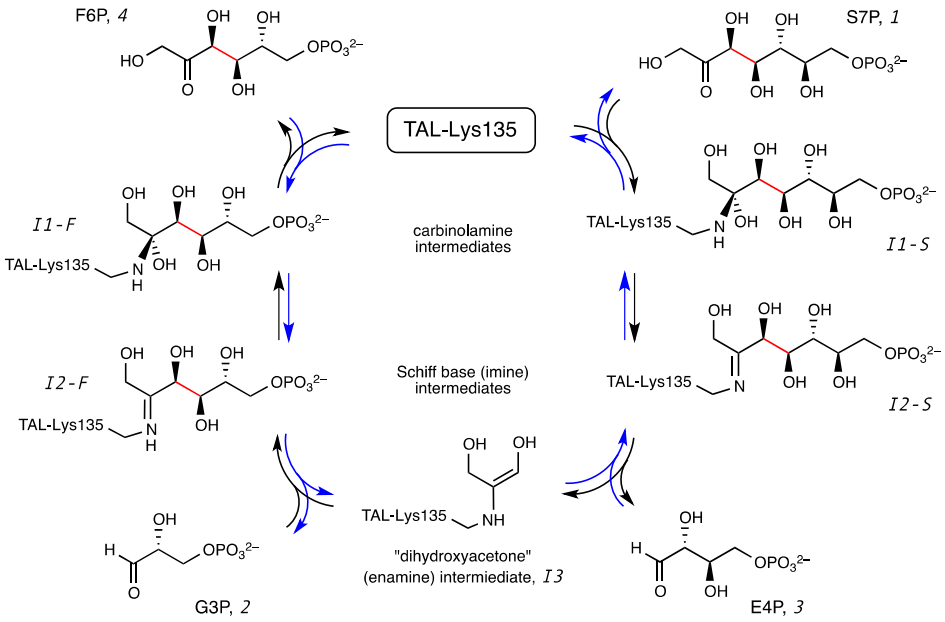

Figure S1. Detailed rendering of the TAL catalytic cycle. Shown here are the individual chemical transformations leading to discrete chemical intermediates in the transaldolase (TAL) catalytic cycle. Comparable intermediates on the F6P and S7P "arms" of the cycle are comparably labeled, followed by -F or -S suffixes, respectively. Note, the abbreviated version of these transformations presented in **Figure 1** in the main text combines related intermediates *I1-F* and *I1-S* as *I1*, and *I2-F* and *I2-S* as *I2*.

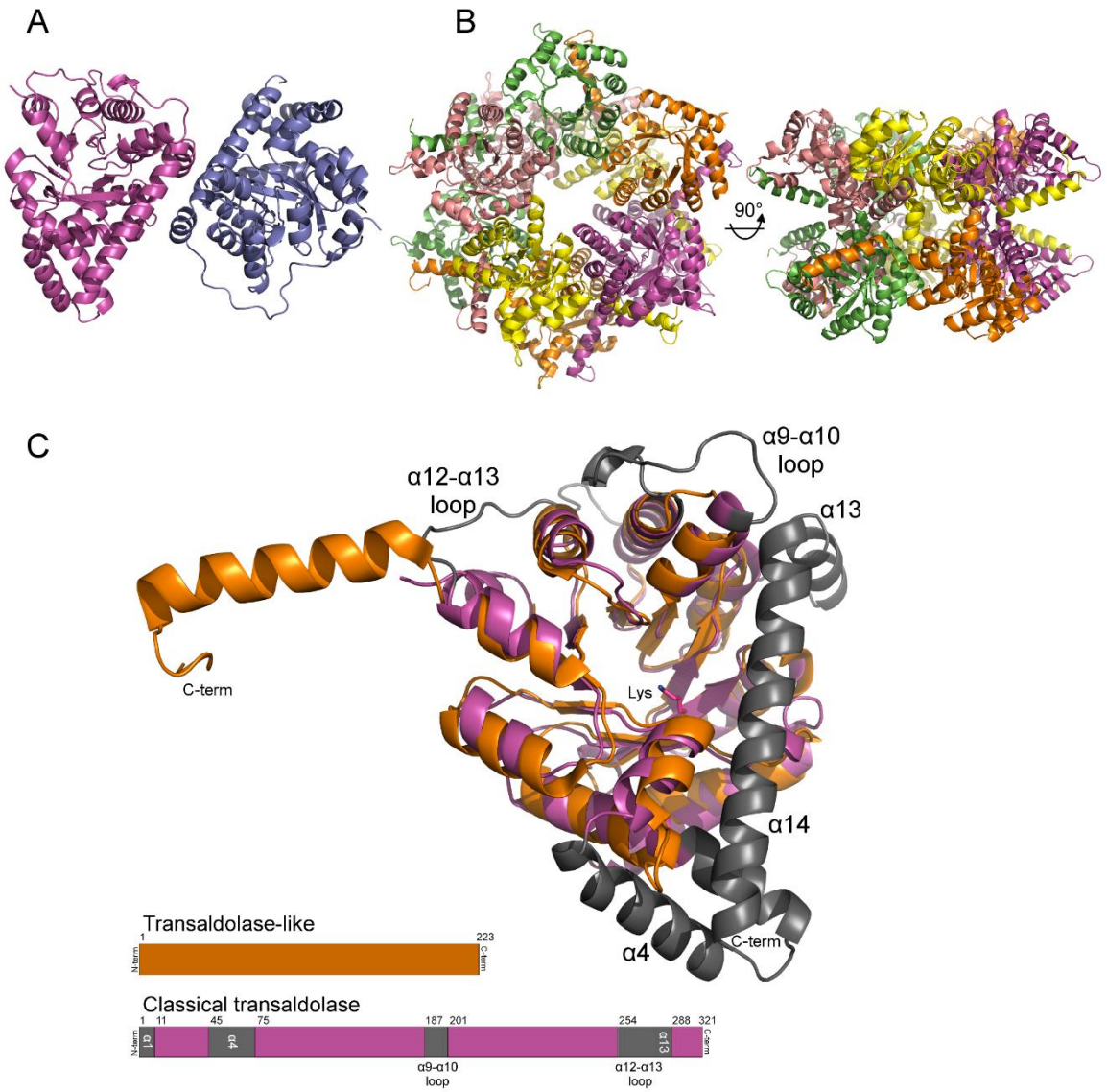

Figure S2. Distinct CT and TLL quaternary structures. (A) The *E. coli* CT (PDB code 1ONR, colored by chain) forms a dimer. (B) The *T. acidophilum* TLL (PDB code 3S0C, colored by chain) forms a pair of pentamer rings (seen in top view) that associate to establish a decamer (seen in lateral view). (C) *T. acidophilum* TLL (PDB code 3S0C) and *E. coli* CT (PDB code 1ONR) structures are superimposed (RMSD = 1.46 over 135 Cα atoms). CT specific insertions are colored gray. Due to inter-subunit helix swapping in the TLL decamer, the C-terminal helix from a neighboring molecule (yellow) superimposes with the CT C-terminal helix. The essential Schiff base forming lysine is shown in stick representation.

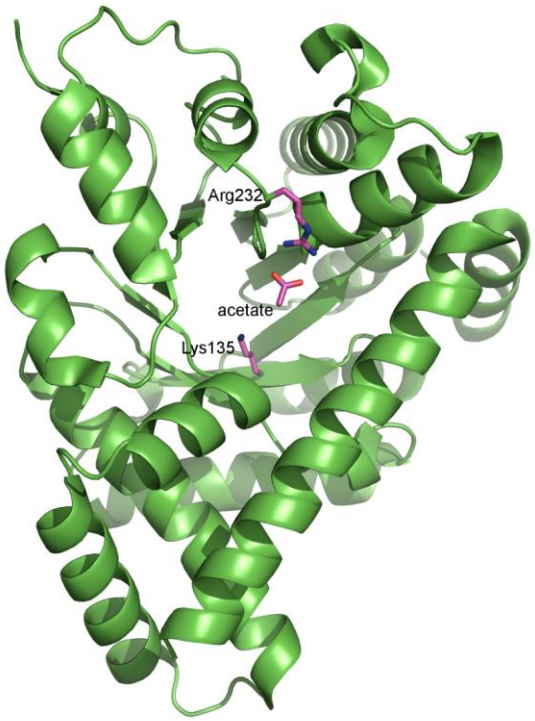

Figure S3. Acetate binding at the active site. An acetate ion is observed at the active site of one of the molecules in the asymmetric unit (purple sticks). Positioned at opposing ends of the active site, Lys135 and Arg232 side chains, are also shown.

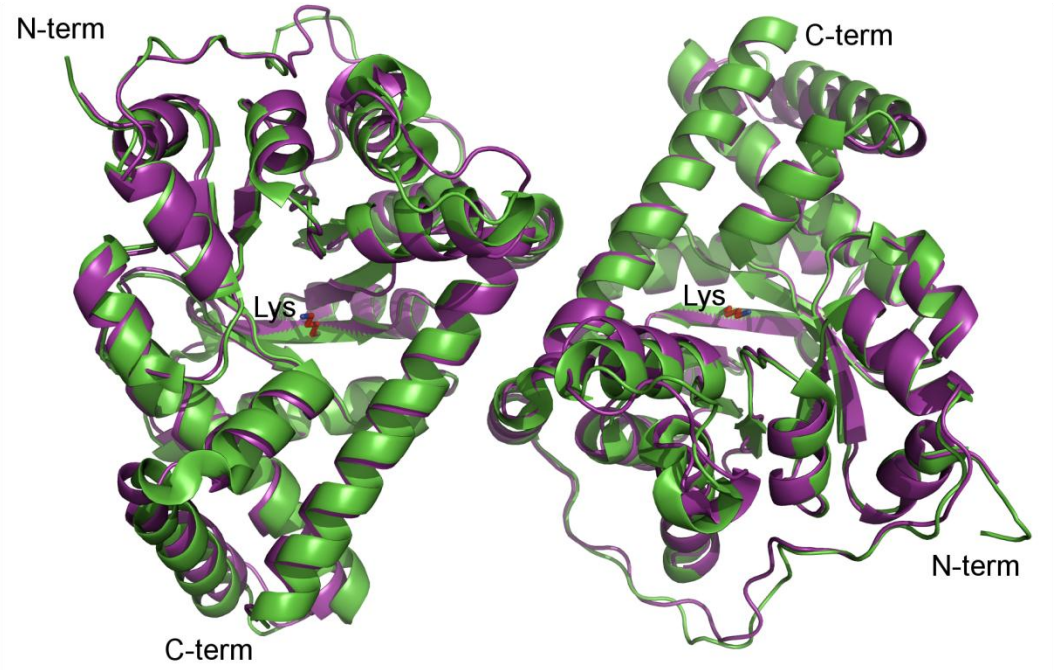

Figure S4. Tertiary and quaternary conservation in CTs. A superposition of *E. coli* (PDB code 3S0C, purple) and *F. tularensis* (green) transaldolase dimers reveals highly similar tertiary and quaternary structures (RMSD = 0.63 over 456 Cα atoms). The quarternary structure is similarly conserved with the human transaldolase (RMSD = 0.54 over 480 Cα atoms). Predicted Schiff base forming lysines are shown as sticks.

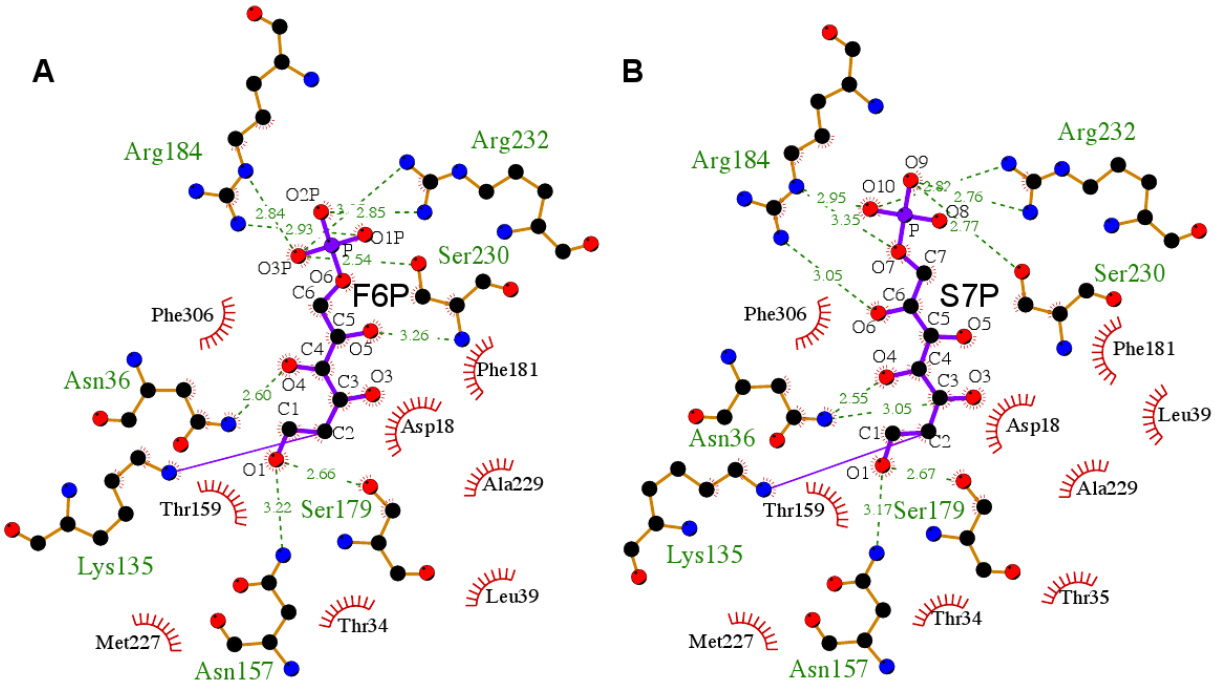

Figure S5. Schematic rendering of protein-ligand interactions in Schiff base complexes. (A) Interactions made by F6P. (B) Interactions made by S7P. Dashed lines indicate hydrogen bonds and red spoke semi-circle indicate hydrophobic contacts. Both panels were generated in LigPlot+ (Laskowski and Swindells, 2011).

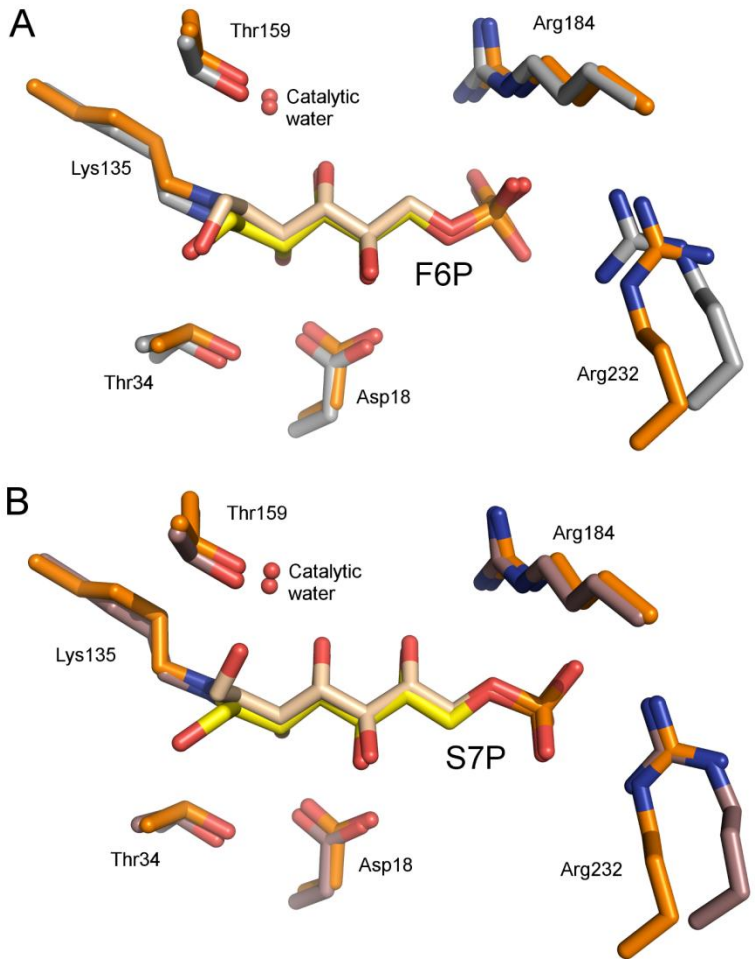

Figure S6. Comparison of *F. tularensis* CT and *T. acidophilum* TLL F6P and S7P complexes. (A) Superposition of CT (gray) and TLL (orange, PDB code 3S1V) F6P complexes. (B) Superposition of CT (violet) and TLL (orange, PDB code 3S1X) S7P complexes. In the TLL structures, the 1-hydroxyl of the sugar adopts two conformations. While only one conformation is shown in each panel, an analysis of the density and B-factors suggests the partial occupancy of each conformation (Lehwess-Litzmann et al., 2011). The 1-hydroxyl conformation shown in the F6P superposition is similar to the conformation of the hydroxyl observed in CT complexes, whereas the 1-hydroxyl conformation shown in the S7P complex is unique to the TLL structures.

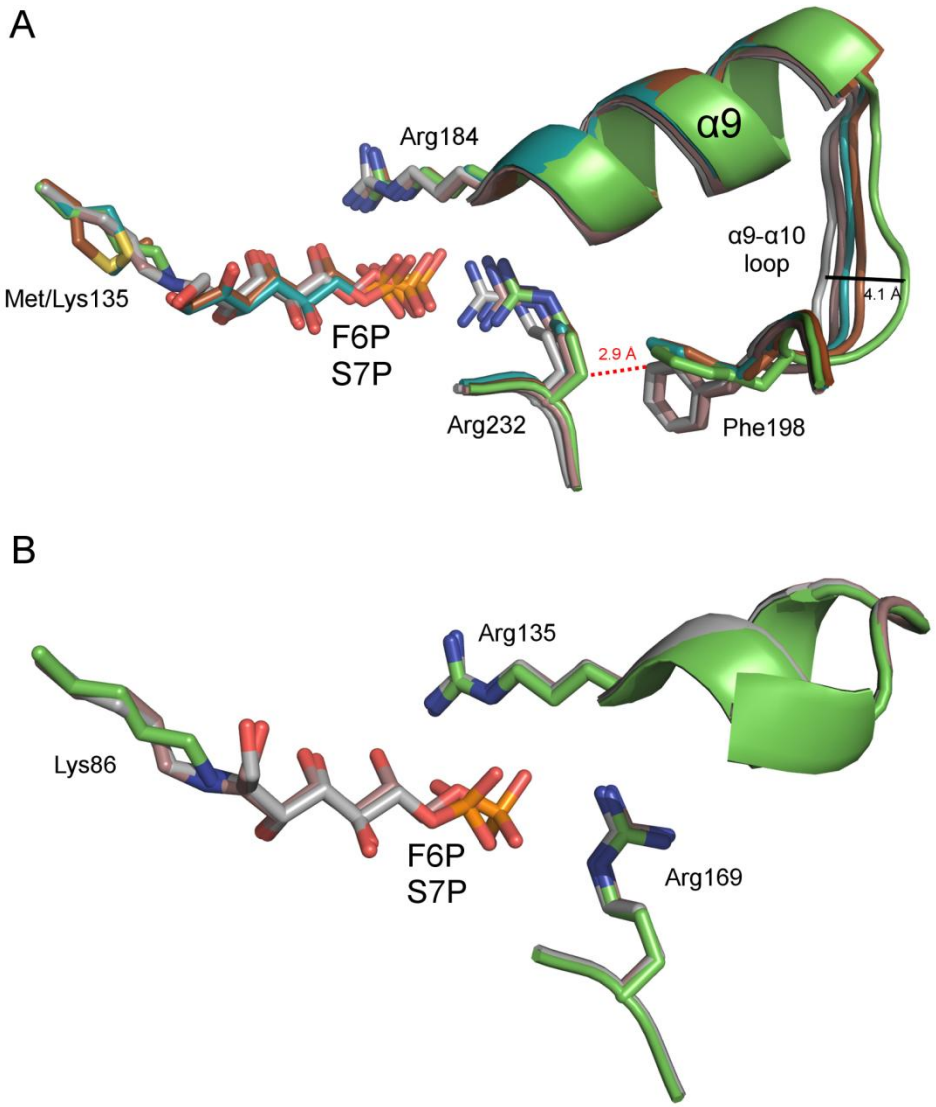

Figure S7. Identification of a CT specific mobile phosphate binding pocket. (A) The unliganded structure (green), F6P (gray) and S7P (violet) Schiff base bound complexes, and K135M mutant F6P (blue) and S7P (brown) complexes are superimposed. The position of the phosphate group depends on the length of the sugar and its non-covalent/covalent binding status. The conformation of Arg232 and the α9-α10 connecting loop correlates with the depth of the phosphate in the active site channel. The loop conformation in the F6P Schiff base complex would sterically clash with the Arg232 unliganded conformation (dashed red line) – a clear indication that loop and Arg232 conformational states are linked. (B) The unliganded (green, PDB code 3S0C), F6P (gray, PDB code 3S1V), and S7P (violet, PDB code 3S1X) Schiff base bound *T. acidophilum* TLL complexes are superimposed and shown from the same perspective as (A). The Arg169 side chain (corresponding to CT Arg232) adopts a different conformation than in CT. As the α9-α10 loop residues represent a CT specific insertion (**Figure S2**), TLL lacks a comparable Arg169 flank. In contrast to CT, sugar binding to TLL is not associated with conformational change of Arg169.

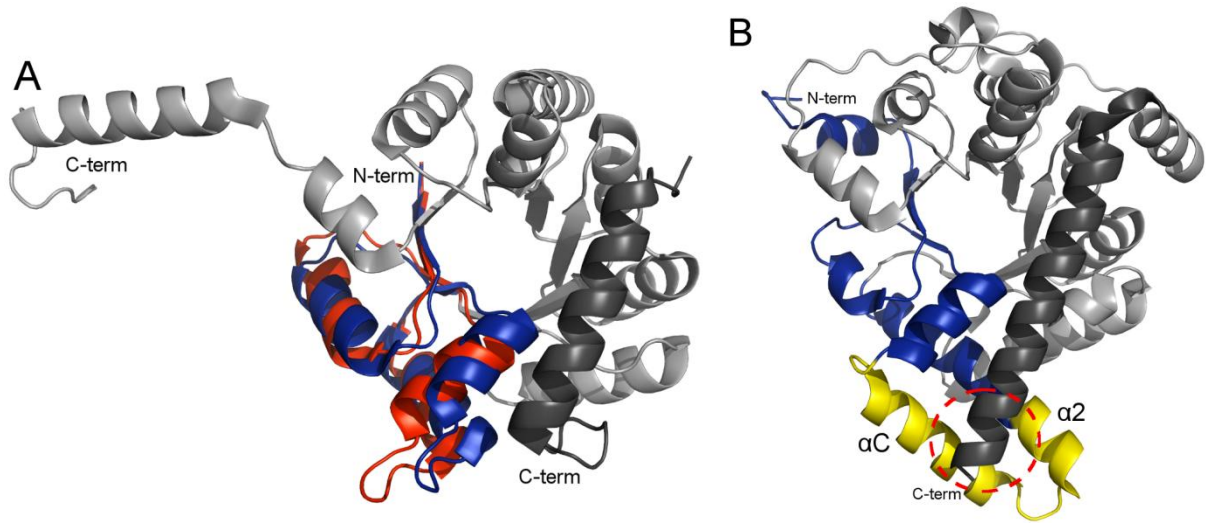

Figure S8. Distinctions in the conformational behavior of CT and TLL N-termi. (A) Superposition of unliganded (PDB code 3S0C) and F6P bound (PDB code 3S1V) structures of *T. acidophilum* TL. The N-terminus adopts an open conformation in the unligande state (red) and a closed conformation in the substrate bound state (blue). (B) The N-terminus of the *F. tularensis* CT (blue) adopts a conformation similar to the closed TLL state. Compared to TL, α2 is extended and αC is unique in CT (yellow). This CT specific appendage engages the extended C-terminal helix (dashed red circle) to form an interaction that may restrict N-terminal mobility and explain the distinct conformational behavior of the two transaldolase types.

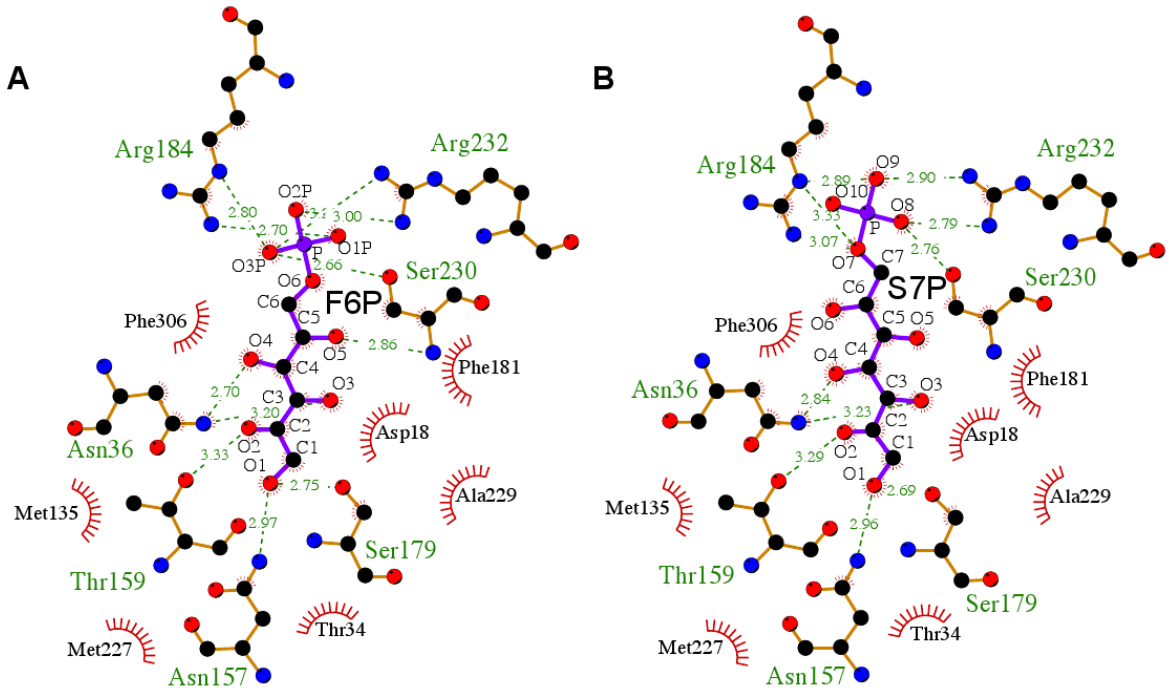

Figure S9. Schematic rendering of protein-ligand interactions in the K135M complexes. (A) Interactions made by F6P. (B) Interactions made by S7P. Dashed lines indicate hydrogen bonds and red spoke semi-circle indicate hydrophobic contacts. Both panels were generated in LigPlot+ (Laskowski and Swindells, 2011).

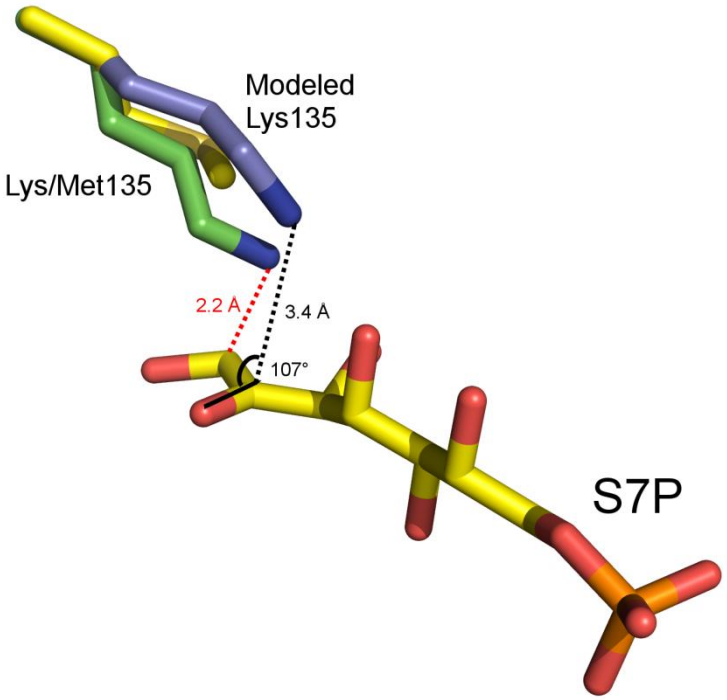

Figure S10. Inferred Lys135 nucleophilic approach. Superposition of unliganded (green) and K135M-S7P complex (yellow). The unliganded conformation of Lys135 would sterically clash with S7P (red dashes). However, a small Lys135 conformational change (blue) could prevent this clash and position the N^{ε} atom at the Bürgi-Dunitz approach angle.

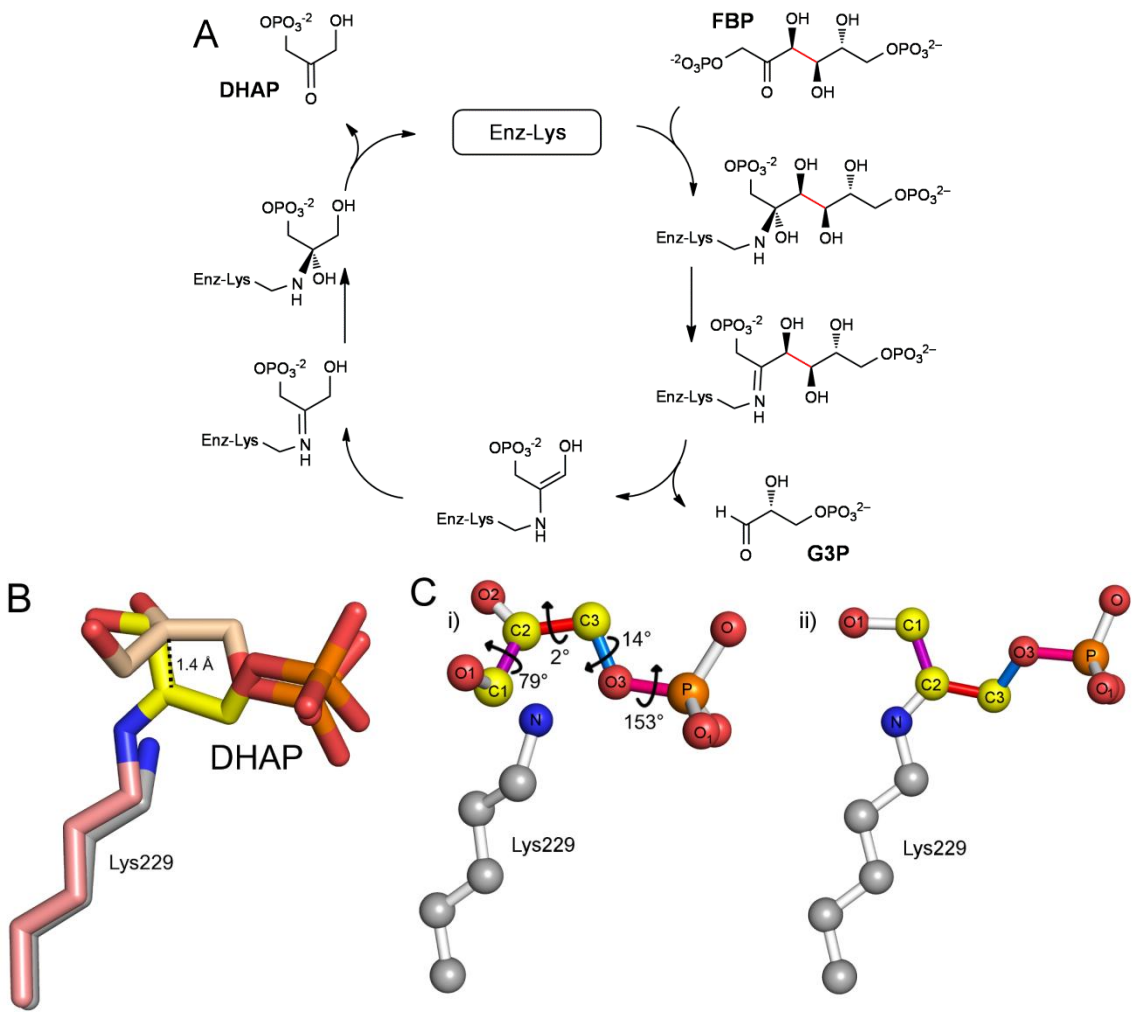

Figure S11. Analysis of fructose 1,6-bisphosphate aldolase Schiff base formation. (A) Schematic rendering of fructose 1,6-bisphosphate aldolase reaction intermediates. The scissile carbon-carbon bond is highlighted in red (B) Superposition of non-covalent (B conformation shown, PDB code 1ADO) and Schiff base bound (K146A mutant, PDB code 2QUU) phosphate-dihyroxyacetone complexes. In the non-covalent complex the N^{ε} atom of the lysine approaches 107° from the plane of the carbonyl bond. (C) Schematic representation of the two complexes highlighting the transformation in bond dihedrals that occurs over the course of Schiff base formation. Like transaldolase, bond formation is associated with changes in substrate dihedral angles. Differences in (i) non-covalent and (ii) covalent conformational states result from rotations around bond dihedrals: $\angle O^1\text{-}C^1\text{-}C^2\text{-}O^2$ (purple), $\angle O^2\text{-}C^2\text{-}C^3\text{-}O^3$ (red), $\angle C^2\text{-}C^3\text{-}O^3\text{-}P$ (marine), $\angle C^3\text{-}O^3\text{-}P\text{-}O_1$ (pink).

Supporting References

Laskowski, R.A., and Swindells, M.B. (2011). LigPlot+: multiple ligand-protein interaction diagrams for drug discovery. J Chem Inf Model *51*, 2778-2786.
Lehwess-Litzmann, A., Neumann, P., Parthier, C., Ludtke, S., Golbik, R., Ficner, R., and Tittmann, K. (2011). Twisted Schiff base intermediates and substrate locale revise transaldolase mechanism. Nat Chem Biol *7*, 678-684.
Watt, W.B., and Dean, A.M. (2000). Molecular-functional studies of adaptive genetic variation in prokaryotes and eukaryotes. Annu Rev Genet *34*, 593-622.